LETTERS
PUBLISHED ONLINE: 2 JULY 2013 | DOI: 10.1038/NCLIMATE1936
nature climate change

El Niño modulations over the past seven centuries

Jinbao Li[1,2]*, Shang-Ping Xie[2,3,4], Edward R. Cook[5], Mariano S. Morales[6], Duncan A. Christie[7,8], Nathaniel C. Johnson[2], Fahu Chen[9], Rosanne D'Arrigo[5], Anthony M. Fowler[10], Xiaohua Gou[9] and Keyan Fang[9]

Predicting how the El Niño/Southern Oscillation (ENSO) will change with global warming is of enormous importance to society[1–4]. ENSO exhibits considerable natural variability at interdecadal–centennial timescales[5]. Instrumental records are too short to determine whether ENSO has changed[6] and existing reconstructions are often developed without adequate tropical records. Here we present a seven-century-long ENSO reconstruction based on 2,222 tree-ring chronologies from both the tropics and mid-latitudes in both hemispheres. The inclusion of tropical records enables us to achieve unprecedented accuracy, as attested by high correlations with equatorial Pacific corals[7,8] and coherent modulation of global teleconnections that are consistent with an independent Northern Hemisphere temperature reconstruction[9]. Our data indicate that ENSO activity in the late twentieth century was anomalously high over the past seven centuries, suggestive of a response to continuing global warming. Climate models disagree on the ENSO response to global warming[3,4], suggesting that many models underestimate the sensitivity to radiative perturbations. Illustrating the radiative effect, our reconstruction reveals a robust ENSO response to large tropical eruptions, with anomalous cooling in the east-central tropical Pacific in the year of eruption, followed by anomalous warming one year after. Our observations provide crucial constraints for improving climate models and their future projections.

El Niño and La Niña are the warm and cold phases of the ENSO cycle, and have profound impacts on worldwide weather and climate through large-scale, far-reaching patterns known as atmospheric teleconnections[1,2]. State-of-the-art climate models disagree on the nature of ENSO behaviour in a warmer climate[3,4]. ENSO properties, such as amplitude, frequency and associated teleconnection patterns, have undergone considerable natural variability at interdecadal (10–90 years) to centennial (~100 years) timescales[5,10]. Instrumental records, available for only about the past 150 years, are not nearly long enough to capture the full behaviour of ENSO variability[6]. Multiple palaeo-reconstructions of ENSO activity are available (Supplementary Table S1), but they generally cover the past few centuries or non-continuous fractions of the past millennium, and many of them do not represent ENSO variability directly, owing to their strong dependence on extratropical proxy records. To address these challenges, we compile and synthesize 2,222 tree-ring chronologies from both the tropics and mid-latitudes of both hemispheres to reconstruct ENSO variability for the past seven centuries. By consolidating coherent signals in tree rings from such diverse regions, we aim to represent ENSO variability more accurately.

Our tree-ring network is composed of 2,222 chronologies from Asia, New Zealand, and North and South America (Supplementary Table S2). Of these, strong ENSO signals are found in tree rings from seven regions, including two in the tropics (Maritime Continent and South American Altiplano), three in the mid-latitude Northern Hemisphere (Central Asia, southwest North America, and the Pacific Northwest/Texas–Mexico (TexMex) region) and two in the mid-latitude Southern Hemisphere (northern New Zealand and west-central Argentina; Fig. 1a). We extract regional variability from tree rings by either a principal components analysis or the development of a regional chronology (Supplementary Methods). The resultant seven time series, one from each region, serve as the basis for our ENSO reconstruction. The first principal component (PC1) of the seven time series, covering the period 1301–1992 and explaining 26.6% of the total variance, is highly correlated with tropical Pacific sea surface temperatures[11] (SSTs; Fig. 1a). PC1 correlates highly with the previous November–January (NDJ) Niño3.4 index ($r = 0.80$) during 1871–1992. The correlation with the trans-Niño index[12], a measure of the zonal SST gradient, is statistically significant but much lower ($r = -0.43$), suggesting that the tree rings are most sensitive to east-central tropical Pacific SST anomalies instead of their east–west gradient. Therefore, we develop a reconstruction for the canonical ENSO variability (Methods and Supplementary Fig. S1), as represented by the Niño3.4 index (Fig. 1b).

Our reconstruction is highly correlated with existing ENSO records, whether their input data are completely independent or with a few overlapping subsets (Supplementary Table S1). Compared with other reconstructions, ours incorporates tree rings from two tropical regions that have higher weights in the empirical orthogonal function than the extratropical peers (Supplementary Table S2), leading to a roughly 10% increase in explained instrumental ENSO variance (Supplementary Table S1). To further verify the reconstruction, we compare it with independent records from the equatorial Pacific. The Southern Oscillation Index[13] (SOI) is a standardized index of sea level pressure difference between Tahiti and Darwin, Australia (Fig. 1a), and represents the atmospheric component of ENSO. Our reconstruction correlates at -0.67 ($P < 0.001$) with the boreal winter (September–February) SOI for their common period 1867–2005 (Fig. 1c), close to the correlation between instrumental Niño3.4 SST and SOI indices for the same period ($r = -0.83$). Our reconstruction is significantly

[1]Department of Geography, University of Hong Kong, Hong Kong, [2]International Pacific Research Center, University of Hawaii at Manoa, Honolulu, Hawaii 96815, USA, [3]Scripps Institution of Oceanography, University of California at San Diego, La Jolla, California 92093-0230, USA, [4]Physical Oceanography Laboratory and Ocean–Atmosphere Interaction and Climate Laboratory, Ocean University of China, Qingdao 266100, China, [5]Lamont-Doherty Earth Observatory, Columbia University, Palisades, New York 10964, USA, [6]Instituto Argentino de Nivología, Glaciología y Ciencias Ambientales (IANIGLA), CCT-CONICET, C.C. 330, 5500 Mendoza, Argentina, [7]Laboratorio de Dendrocronología y Cambio Global, Instituto de Conservación Biodiversidad y Territorio, Facultad de Ciencias Forestales y Recursos Naturales, Universidad Austral de Chile, Casilla 567, Valdivia, Chile, [8]Center for Climate and Resilience Research [CR]², Casilla 2777, Chile, [9]MOE Key Laboratory of Western China's Environmental System, Lanzhou University, Lanzhou 730000, China, [10]School of Environment, The University of Auckland, Auckland 1020, New Zealand. *e-mail: jinbao@hku.hk

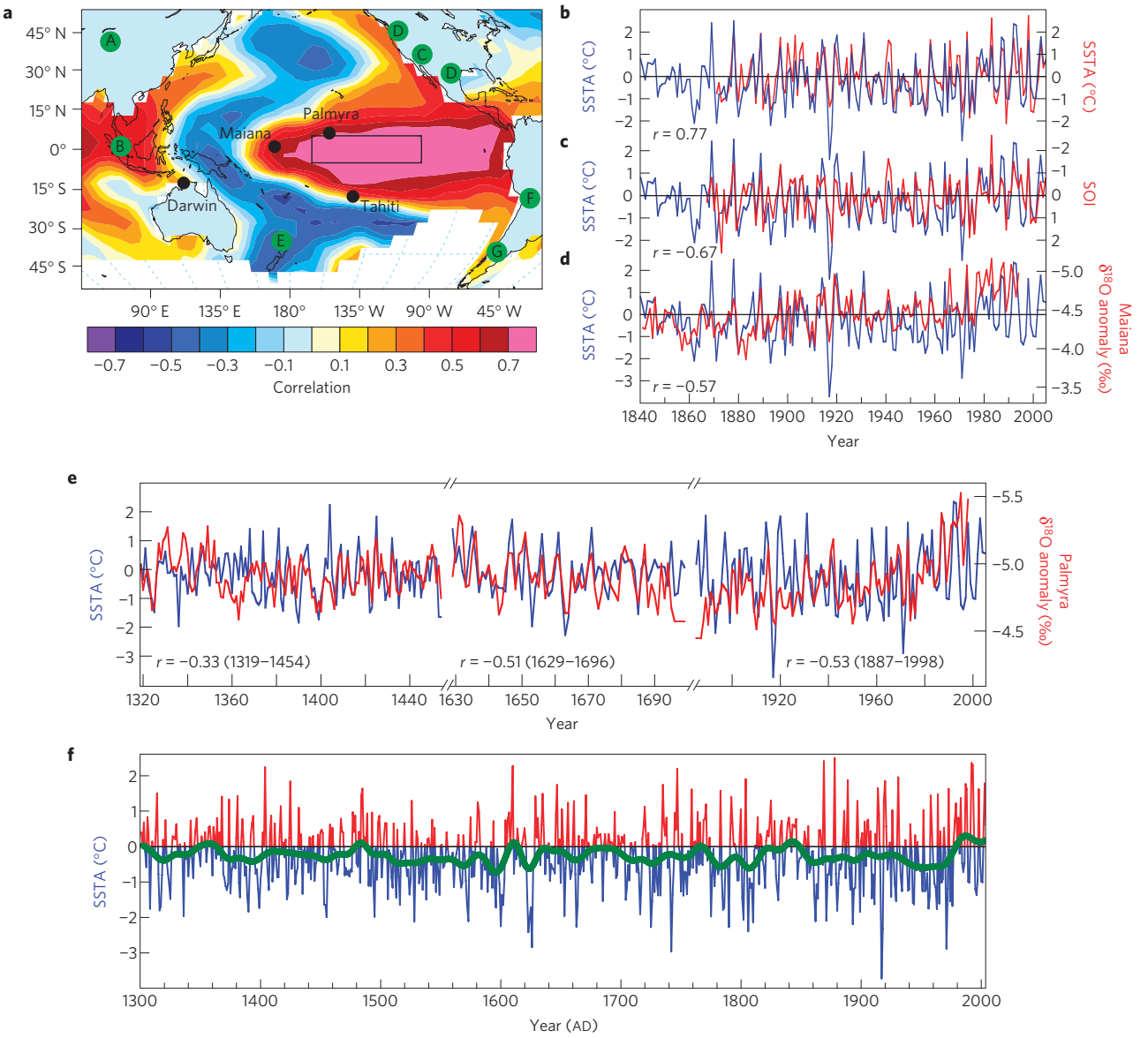

Figure 1 | ENSO reconstruction and verification. a, Spatial correlation field of tree-ring PC1 with global NDJ SSTs (ref. 11) during 1871–1992. The black rectangle denotes the Niño3.4 region. The shaded letters denote areas where tree rings are sensitive to ENSO (Supplementary Table S2). The black dots indicate site locations mentioned in the text. **b**–**e**, Comparison of our ENSO reconstruction (blue) with tropical records (red). **b**, NDJ instrumental Niño3.4 index during 1871–2005. **c**, Boreal winter (September–February) instrumental SOI during 1867–2005. **d**, Maiana coral $\delta^{18}O$ series[7] during 1841–1994. **e**, Palmyra coral $\delta^{18}O$ series[8] for non-continuous fractions of the past seven centuries. **f**, The reconstructed NDJ Niño3.4 SSTs over 1301–2005. SST anomalies (SSTAs) are relative to the mean of observed SSTs during 1971–2000. The green bold line denotes a 31-yr low-pass filter.

correlated with modern coral records in the central tropical Pacific: $r = -0.57$ ($P < 0.001$) at Maiana Atoll[7] for 1841–1994 (Fig. 1d), and $r = -0.53$ ($P < 0.001$) at Palmyra Island[8] for 1887–1998 (Fig. 1e). After adjusting relict coral U/Th dates within the analytical error windows[5], we find that significant correlations between our reconstruction and Palmyra corals have persisted throughout the past seven centuries (Fig. 1e). The above agreements are remarkable in that these proxy records are completely independent, indicating high fidelity of our reconstruction over the past seven centuries.

The reconstructed ENSO index exhibits marked variations at interannual to interdecadal timescales over the past seven centuries (Fig. 1f). The multi-taper method[14] spectral analysis reveals that significant ENSO periodicities fall within interannual (2–7 years) and decadal (8–13 years) bands, respectively (Supplementary Fig. S2a). The interannual cycles are observed for the instrumental era, a period when the decadal cycles are less pronounced (Supplementary Fig. S3). The time–space wavelet analysis[15] shows that the interannual variability has persisted throughout the past seven centuries, whereas the decadal variability weakens during most of the sixteenth and twentieth century (Supplementary Fig. S2b). Marked decadal variability is also widely found in Indo-Pacific corals in the late nineteenth century, with its spatial pattern closely resembling that of interannual variability[16]. Together these results suggest that decadal variability is a significant component of the ENSO system and is underestimated by instrumental data. We have investigated the relationship between the decadal variability and sunspot number using a cross-wavelet transform (Supplementary Methods). There is a strong spectral coherence but the phase varies by 180° over the course of their common period (Supplementary Fig. S4). If the 11-year solar cycle is linked to decadal ENSO variability, then the mechanism must be able to accommodate meandering 180° phase reversals through time, and has not yet been

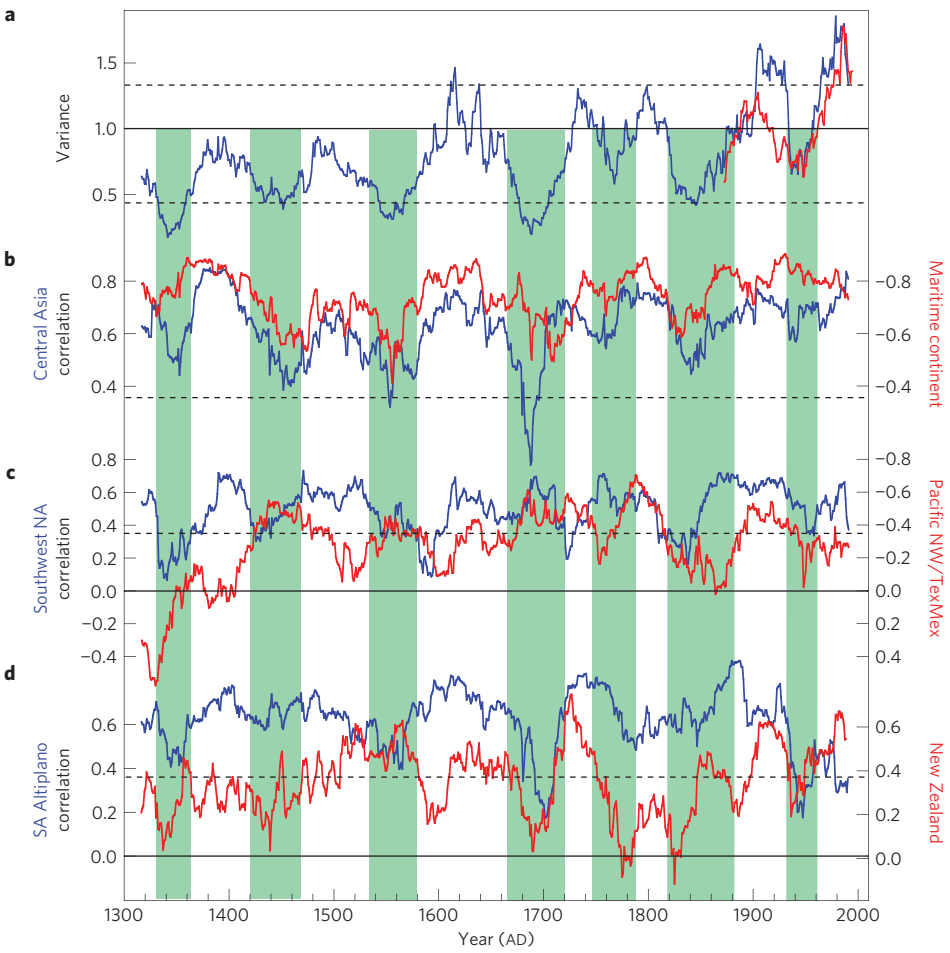

Figure 2 | Modulation of ENSO teleconnections. a, 31-yr running biweight variance for observed (red) and reconstructed (blue) Niño3.4 SSTs. The dashed lines indicate the 95% confidence interval for stochastic variations, based on 10,000 Monte Carlo simulations (Supplementary Methods). **b**–**d**, 31-yr running correlations of reconstructed Niño3.4 SSTs with tree-ring series from Central Asia (blue) and Maritime Continent (red) (**b**), southwest North America (blue) and the Pacific Northwest/TexMex region (red) (**c**), and the South American Altiplano (blue) and northern New Zealand (red) (**d**). The dashed lines in **b**–**d** indicate the 0.05 significance level. Vertical shading denotes periods of low ENSO variance.

determined through climate modelling studies. Instead, decadal ENSO variability more likely results from internal dynamics.

The temporal evolution of ENSO variance represented by our reconstruction is most consistent with that shown by the two tropical records (Supplementary Fig. S5). The mutual agreement between the two independent tropical records suggests that our reconstruction represents ENSO variance more accurately than previous ones that generally do not incorporate tropical records. Overall, the reconstructed ENSO variance was weak in the early Little Ice Age (LIA) of 1300s–1550s, increased during the late LIA of 1550s–1880s, and became unusually high after the 1880s (Fig. 2a). The reconstruction also exhibits larger variance than the instrumental target in the early twentieth century. The empirical reconstructions may underestimate SST variability owing to the lack of observations in that period[2].

The reconstructed ENSO variance exhibits substantial modulation at interdecadal to centennial timescales (Fig. 2a). Such modulation, however, may arise stochastically and thus may not be indicative of dynamics with intrinsic interdecadal timescales[17,18]. We estimate the expected range of variability of 31-yr running biweight variance that may arise stochastically through a Monte Carlo approach (Supplementary Methods). The results indicate that the interdecadal modulation of ENSO variance before 1900 may arise stochastically (Fig. 2a). The running variance during much of the twentieth century, however, exceeds the 95% confidence interval for stochastic variations, suggesting that the recent enhancement of ENSO variance is due to changes in the background state such as the secular positive trend in tropical SSTs (ref. 19). Climate models disagree on the ENSO response to global warming, splitting between enhanced and damped variability[3,4]. Our observations suggest that models with a damped response may underestimate the sensitivity of ENSO to increasing anthropogenic radiative forcing, although significant ENSO changes may still be difficult to detect for periods of less than a century[6]. Regardless, a more thorough attribution of interdecadal ENSO variability in future work requires the combination of developments in theory, coupled climate model simulations, and long records of ENSO variability such as ours.

Determining the strength of ENSO teleconnections is crucial for climate forecasts outside the tropical Pacific. Instrumental records show substantial modulation of ENSO teleconnections on interdecadal timescales during the twentieth century[10,20], but the cause of such modulation remains unclear. Here we calculate 31-year running correlations between the reconstruction and each input series to assess the stationarity of ENSO teleconnections over the pan-Pacific regions for the past seven centuries. The ENSO influence is most robust over the Maritime Continent (Fig. 2b), perhaps not surprisingly as it is a centre of action for ENSO with strong rainfall variability. The ENSO teleconnection is also robust over Central Asia, except for marked reduction within the Maunder minimum of the 1660s–1700s (Fig. 2b). Marked reduction in the

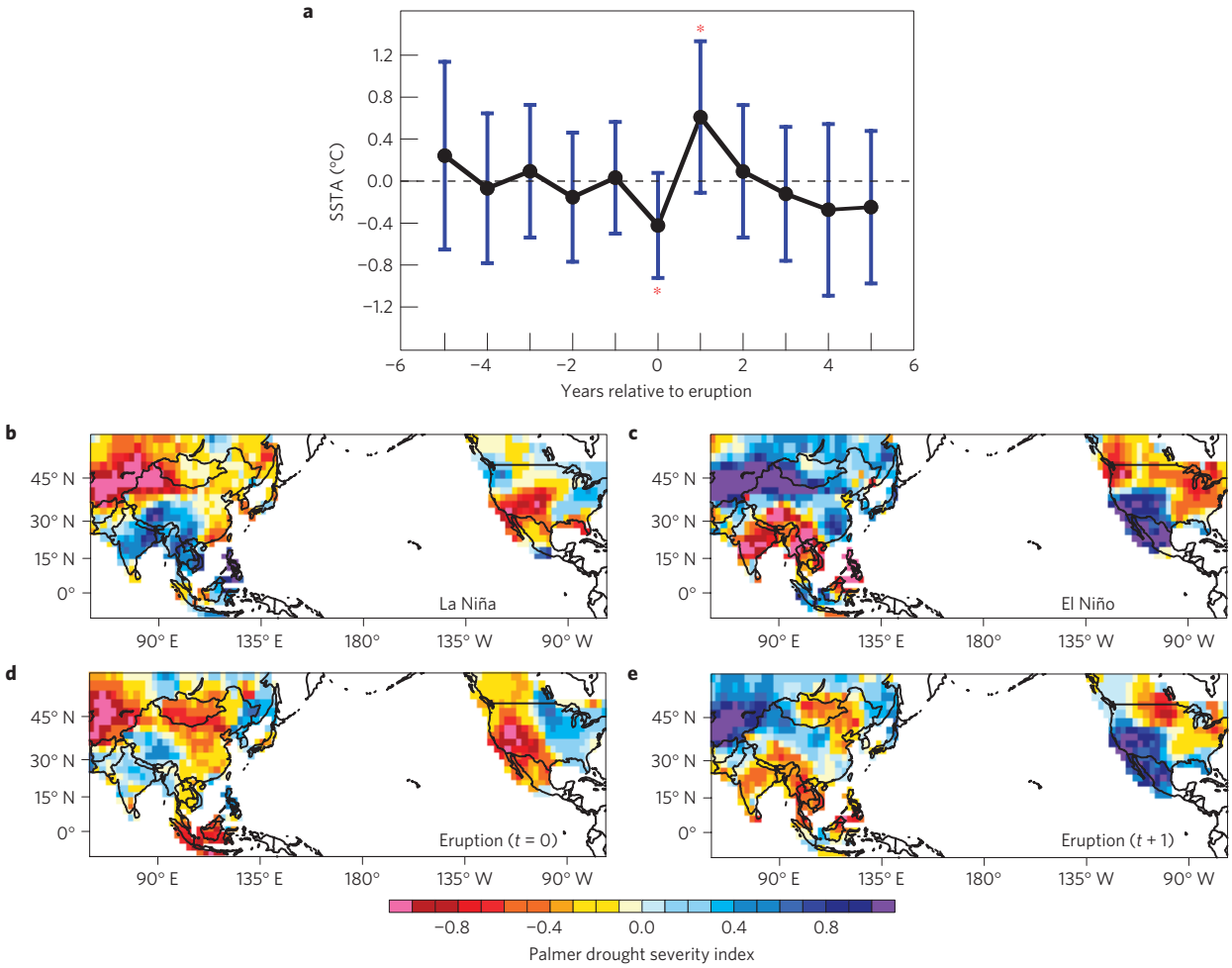

Figure 3 | ENSO response to large tropical eruptions. a, SEA (ref. 22) for large tropical eruptions during 1301–2005. Before the SEA, the reconstructed Niño3.4 SSTs were processed using a 9-yr high-pass filter to isolate interannual variability. Error bars denote SST anomalies of one standard deviation at each year. Asterisks denote anomalies significant at the 0.01 level, based on a two-tailed Student's *t*-test. **b**–**e**, Composite moisture anomalies associated with La Niña (**b**), El Niño (**c**), large tropical eruptions at $t=0$ (**d**) and large tropical eruptions at $t+1$ (**e**). The El Niño (15) and La Niña (19) events are defined as the NDJ SST anomalies exceeding 0.5 °C, using the 9-yr high-pass-filtered Niño3.4 index[11] during 1950–2005 (Supplementary Table S6). The number of large tropical eruptions for composite analysis is 22 (Supplementary Table S4). Moisture conditions are indicated by the Palmer drought severity index[30]. Positive (negative) anomalies indicate wet (dry) conditions, respectively.

strength of ENSO teleconnections during the Maunder minimum is also found over the South American Altiplano and northern New Zealand (Fig. 2d), but not over western North America (Fig. 2c). Overall, ENSO teleconnections are robust over the South American Altiplano and southwest North America for most of the past seven centuries, but vary substantially over northern New Zealand and the Pacific Northwest/TexMex region (Fig. 2c,d). Relative to the ENSO variance time series, we find that ENSO teleconnections over the pan-Pacific regions are generally strong (weak) when the ENSO variance is high (low), with each high/low-variance epoch lasting for several decades (Fig. 2a–d). Likewise, we find that ENSO teleconnections on Northern Hemisphere temperature are linked to changes in ENSO variance (Supplementary Methods and Fig. S6). These concomitant changes throughout the past seven centuries indicate that the ENSO effects on extratropical climate are modulated by ENSO variance at interdecadal to centennial timescales.

Explosive volcanic eruptions affect the climate by injecting aerosols into the atmosphere[21], but their effect on ENSO remains uncertain, with inconclusive results from short observations[21–23] and contradictory results from model simulations[24–26]. Here we use superposed epoch analysis[22] (SEA) to assess their relationship for the past seven centuries. We employ a historical/geological record-based volcanic explosivity index[27] (VEI), which more accurately records eruption location than other indices derived from polar ice core chemistry (Supplementary Table S4). Using a series of sensitivity tests, the results indicate a robust ENSO response to large tropical eruptions (VEI > 4; 22 events), but not to medium eruptions (VEI = 4; 68 events; Supplementary Table S5). For large tropical eruptions, immediate cooling tends to occur in the east-central tropical Pacific in the year of eruption ($t=0$), followed by anomalous warming one year after (Fig. 3a). On average, the Niño3.4 SST difference from year $t=0$ to year $t+1$ amounts to ~1.0 °C, statistically significant at the 0.01 level, based on a two-tailed Student's *t*-test.

Previous studies using shorter and less reliable ENSO reconstructions yielded only a vague picture of a multi-year warming response to a large tropical eruption[22–25]. Our analysis, based on a longer and more accurate ENSO reconstruction, reveals a much richer evolution. An intermediate climate model simulates the subsequent warming through an ocean dynamical thermostat mechanism[28], but not the initial cooling response[24,25]. A recent study using a fully coupled general circulation model suggests a concurrent cooling response to volcanic forcing[26]. Our

observations now offer support for the general circulation model result, suggesting that in addition to the thermostat mechanism, other dynamical processes such as zonal variations in SST damping are important for simulating the full response of ENSO to radiative forcing perturbations.

Did large tropical eruptions cause moisture extremes recorded in tree rings by direct radiative forcing or through the effects on ENSO? To answer this question, we compare volcanically induced moisture anomaly patterns to those of ENSO. The close resemblance of the moisture pattern at year $t = 0$ ($t + 1$) to that of La Niña (El Niño) provides strong evidence that tropical eruptions affect global moisture largely through the influence on ENSO (Fig. 3b–e).

In summary, our tree-ring-based ENSO reconstruction for the past seven centuries represents a major improvement over previous efforts, made possible by including records from the tropics. Our results show marked interdecadal–centennial variations in ENSO amplitude that modulate its effects on extratropical climate, suggesting that ENSO variance, rather than alternative mechanisms such as mid-latitude waveguide modulation[29], is a primary control of the modulations. On longer timescales, ENSO variance is low in the early LIA period and high in the twentieth century. The elevated ENSO variability in recent decades is unprecedented over the past seven centuries, suggesting a response to increased anthropogenic radiative forcing. Climate models disagree on the response to global warming, suggesting that many of them may underestimate ENSO sensitivity to radiative perturbations. Although ENSO is an internal mode of the coupled system, our analysis with a large sample size reveals a robust response to large tropical volcanic eruptions. Large tropical eruptions force the Pacific immediately into an anomalous cooling state, followed by anomalous warming in the next year. The response to the 11-year solar cycle is inconsistent in phase over the record, possibly because of weak forcing. This underlines the complexity of ENSO dynamics and calls for further investigations into the sensitivity to the magnitude and timescale[19] of radiative forcing. Regardless, the robust ENSO response to volcanic forcing, and in particular its evolution in time, offers an excellent test bed for climate models if they are to yield future projections with confidence.

Methods

We developed an ENSO reconstruction with a well-tested principal components regression procedure (see Supplementary Methods). The PC1 of the tree-ring records was retained to build a linear regression model by calibrating on the NDJ Niño3.4 index during 1871–1992. The reconstruction was extended to 2005 with a nested approach, with two iterative regression nests ending in 2003 (six input series) and 2005 (five input series). We performed rigorous calibration and verification tests, and the results indicate significant skill in all three regression models (Supplementary Fig. S1 and Table S3). The final reconstruction was achieved by merging the three regressions together, with their mean and variance adjusted to be the same as the 1301–1992 nest. The final reconstruction accounts for 63.5% of instrumental Niño3.4 SST variance during 1871–1992 (Fig. 1b).

Received 13 November 2012; accepted 28 May 2013; published online 2 July 2013

References

1. McPhaden, M. J., Zebiak, S. E. & Glantz, M. H. ENSO as an integrating concept in earth science. *Science* **314,** 1740–1745 (2006).
2. Deser, C., Alexander, M. A., Xie, S.-P. & Phillips, A. S. Sea surface temperature variability: Patterns and mechanisms. *Annu. Rev. Mar. Sci.* **2,** 115–143 (2010).
3. Guilyardi, E. *et al.* Understanding El Niño in ocean–atmosphere general circulation models: Progress and challenges. *Bull. Am. Meteorol. Soc.* **90,** 325–340 (2009).
4. Collins, M. *et al.* The impact of global warming on the tropical Pacific Ocean and El Niño. *Nature Geosci.* **3,** 391–397 (2010).
5. Li, J. *et al.* Interdecadal modulation of El Niño amplitude during the past millennium. *Nature Clim. Change* **1,** 114–118 (2011).
6. Stevenson, S. *et al.* Will there be a significant change to El Nino in the 21st century? *J. Clim.* **25,** 2129–2145 (2012).
7. Urban, F. E., Cole, J. E. & Overpeck, J. T. Influence of mean climate change on climate variability from a 155-year tropical Pacific coral record. *Nature* **407,** 989–993 (2000).
8. Cobb, K. M., Charles, C. D., Cheng, H. & Edwards, R. L. El Niño/Southern Oscillation and tropical Pacific climate during the last millennium. *Nature* **424,** 271–276 (2003).
9. Mann, M. E., Bradley, R. S. & Hughes, M. K. Northern Hemisphere temperatures during the past millennium: Inferences, uncertainties, and limitations. *Geophys. Res. Lett.* **26,** 759–762 (1999).
10. Chowdary, J. S. *et al.* Inter-decadal variations in ENSO teleconnection to the Indo-western Pacific for 1870–2007. *J. Clim.* **25,** 1722–1744 (2012).
11. Kaplan, A. *et al.* Analyses of global sea surface temperature 1856–1991. *J. Geophys. Res.* **103,** 18567–18589 (1998).
12. Trenberth, K. E. & Stepaniak, D. P. Indices of El Niño evolution. *J. Clim.* **14,** 1697–1701 (2001).
13. Ropelewski, C. F. & Jones, P. D. An extension of the Tahiti–Darwin southern oscillation index. *Mon. Weath. Rev.* **115,** 2161–2165 (1987).
14. Mann, M. E. & Lees, J. Robust estimation of background noise and signal detection in climatic time series. *Climatic Change* **33,** 409–445 (1996).
15. Torrence, C. & Compo, G. P. A practical guide to wavelet analysis. *Bull. Am. Meteorol. Soc.* **79,** 61–78 (1998).
16. Ault, T. R. *et al.* Intensified decadal variability in tropical climate during the late 19th century. *Geophys. Res. Lett.* **36,** L08602 (2009).
17. Wittenberg, A. T. Are historical records sufficient to constrain ENSO simulations? *Geophys. Res. Lett.* **36,** L12702 (2009).
18. Gershunov, A., Schneider, N. & Barnett, T. Low-frequency modulation of the ENSO-Indian monsoon rainfall relationship: Signal or noise? *J. Clim.* **14,** 2486–2492 (2001).
19. Emile-Geay, J., Cobb, K., Mann, M. & Wittenberg, A. T. Estimating central equatorial Pacific SST variability over the past millennium. Part 2: Reconstructions and uncertainties. *J. Clim.* **26,** 2329–2352 (2013).
20. Gershunov, A. & Barnett, T. P. Interdecadal modulation of ENSO teleconnections. *Bull. Am. Meteorol. Soc.* **79,** 2715–2726 (1998).
21. Robock, A. Volcanic eruptions and climate. *Rev. Geophys.* **38,** 191–219 (2000).
22. Adams, J. B., Mann, M. E. & Ammann, C. M. Proxy evidence for an El Niño-like response to volcanic forcing. *Nature* **426,** 274–278 (2003).
23. D'Arrigo, R., Wilson, R. & Tudhope, A. Impact of volcanic forcing on tropical temperatures during the last four centuries. *Nature Geosci.* **2,** 51–56 (2009).
24. Mann, M. E., Cane, M. A., Zebiak, S. E. & Clement, A. Volcanic and solar forcing of the tropical Pacific over the past 1000 years. *J. Clim.* **18,** 447–456 (2005).
25. Emile-Geay, J., Seager, R., Cane, M. A., Cook, E. R. & Haug, G. H. Volcanoes and ENSO over the past millennium. *J. Clim.* **21,** 3134–3148 (2008).
26. McGregor, S. & Timmermann, A. The response of ENSO to explosive volcanic eruptions. *J. Clim.* **24,** 2178–2191 (2011).
27. Siebert, L. & Simkin, T. *Volcanoes of the World: An Illustrated Catalog of Holocene Volcanoes and Their Eruptions* (Global Volcanism Program Digital Information Series, Smithsonian Institution, GVP-3, 2012).
28. Clement, A. C., Seager, R., Cane, M. A. & Zebiak, S. E. An ocean dynamical thermostat. *J. Clim.* **9,** 2190–2196 (1996).
29. Kang, I-S. Influence of zonal mean flow change on stationary wave fluctuations. *J. Atmos. Sci.* **47,** 141–147 (1990).
30. Palmer, W. C. *Meteorological Drought* (US Department of Commerce, 1965).

Acknowledgements

We thank the researchers who have contributed their tree-ring data for MADA and NADA development, and W. Soon for helpful discussions on the records of sunspot number. This research was financially supported by the National Science Foundation, the National Basic Research Program of China (2012CB955600), the National Oceanic and Atmospheric Administration, the Japan Agency for Marine-Earth Science and Technology, FONDECYT (No.1120965), CONICYT/FONDAP/15110009, CONICET and IAI (CRN2047). This is an International Pacific Research Center/School of Ocean and Earth Science and Technology Contribution (987/8948) and a Lamont–Doherty Earth Observatory Contribution (7699).

Author contributions

J.L., S-P.X. and E.R.C. designed the research. J.L., S-P.X., M.S.M., D.A.C. and N.C.J. analysed data. J.L., S-P.X. and N.C.J. wrote the paper. All authors discussed the results and commented on the manuscript.

Additional information

Supplementary information is available in the online version of the paper. Reprints and permissions information is available online at www.nature.com/reprints. Correspondence and requests for materials should be addressed to J.L.

Competing financial interests

The authors declare no competing financial interests.

nature climate change

SUPPLEMENTARY INFORMATION

DOI: 10.1038/NCLIMATE1936

El Niño modulations over the past seven centuries

Supplementary Methods; Supplementary References; Supplementary Figures and Legends S1–S7; Supplementary Tables S1-S6

This file contains supplementary information for the ENSO reconstruction, decadal ENSO variability, and statistical assessment of interdecadal modulation of ENSO variance (Supplementary Methods, Figs. S1-S7 and Tables S1-S3). Supplementary Table S4 lists large tropical volcanic eruptions during the past seven centuries. Supplementary Table S5 provides sensitivity tests for ENSO response to large tropical eruptions. Supplementary Table S6 lists El Niño and La Niña years during 1950-2005.

DOI: 10.1038/NCLIMATE1936

El Niño modulations over the past seven centuries

Supplementary Methods

ENSO reconstruction. Here we use 2222 tree-ring chronologies from both the tropics and mid-latitudes of both hemispheres to reconstruct ENSO variability for the past seven centuries. All chronologies were developed with consistent (and conservative) methods[31] to remove biological growth trends while preserving climate-related variability. Tree-ring indices were calculated as ratios of actual to expected growth. Robust mean chronologies were developed by merging all tree-ring index series for each site. To minimize the potential influence of changing sample size on variance, each chronology was put through a process of variance stabilization, using the technique described in *(32).* The reliability of each chronology was assessed using the expressed population signal (EPS) statistic, and only those chronology periods in which this statistic exceeds a commonly held threshold value of 0.85 were used in this study[33]. These methods have been extensively tested with pseudo-proxy experiments and tree-ring records around the world, and have been proven to effectively minimize the sample size or biological age related tendency in variance[32,34].

There are 327 (1845) tree-ring chronologies across Monsoon Asia (North America), respectively. In order to determine climate signals encoded in these tree-rings, we employed them to develop gridded datasets of boreal summer (June-August) Palmer Drought Severity Index[30] (PDSI) reconstructions, namely, the Monsoon Asia Drought Atlas[35] (MADA) and North America Drought Atlas[36,37] (NADA). We take advantage of MADA and NADA to define the spatially coherent drought patterns over Monsoon Asia

(MA) and North America (NA) for the past seven centuries, and then analyze if temporal changes of each drought pattern are related to ENSO. The results indicate that the first two dominant drought patterns of MADA and NADA, with their centers over Central Asia, Maritime Continent, Southwest NA, and the Pacific Northwest/TexMex region, are all strongly associated with ENSO (*refs. 35, 38*). In addition, we find three regional chronologies, developed with tree-rings from northern New Zealand[39] (38 sites), South American Altiplano[40] (7 sites), and west-central Argentina[41] (5 sites), are also highly related to ENSO. These seven time series, each capturing ENSO teleconnection in its source region, serve as the basis for our reconstruction.

There are two popular methods for proxy-based paleoclimate reconstruction, with one based on the principal components analysis (PCA) and the other using the Regularized Expectation-Maximization (RegEM) technique[42]. The two methods generally exhibit comparable skills on single time series reconstruction[19,43]. Here we favor the PCA- instead of the RegEM-based approach for ENSO reconstruction, because the latter depends critically on the instrumental data[19]. The over-dependence of the RegEM technique on the instrumental target could lead to noticeable bias in reconstruction[19], as the tropical Pacific SSTs before 1950 are not "observed" but mostly reconstructed and subject to large errors[44,45]. In contrast, the PCA-based approach depends more on the characteristics of proxy records and is less sensitive to the instrumental target. As shown below, with the PCA-based approach we produced identical reconstructions with three versions of the SST products (Supplementary Fig. S1).

We performed a nested PC regression to optimize the length of the reconstruction[31,46]. The three nests all start in 1301, but end in 1992, 2003, and 2005, respectively. For each

DOI: 10.1038/NCLIMATE1936

nest, the PCA was performed on the actual predictors, and the first PC was retained to develop a regression model. We note that because tree-rings from three (four) regions are influenced by ENSO events that develop (decay) in the growing season (Supplementary Table S2), we lagged time series from the three regions that record developing ENSO events one year prior to reconstruction, so that they correlate with the same ENSO events as the other four time series. The regression models are all calibrated on the prior November-January (NDJ) Niño3.4 index[11] during 1871-1992, and the fidelity of each model was evaluated by split sample calibration and verification tests[31]. The split calibration/verification periods used are 1871–1930 and 1931–1992 (Supplementary Table S3). Reconstruction validity was assessed using Pearson's correlation coefficient, the reduction of error (RE), the coefficient of efficiency (CE), and sign test (ST) statistics. For the RE and CE, positive value indicates significant model skill, with the CE being the more rigorous of the two[31].

The resulting statistics of split sample calibration/verification tests are shown in Supplementary Table S3. The correlation coefficients for each calibration/verification period are generally above 0.78. The values of the two most rigorous tests of model validation, the RE and CE, are generally within the range of 0.60 to 0.65, indicating significant skill of the regressions. The results of ST, which describes how well the predicted value tracks the sign of actual data, all exceed the 0.001 significance level. Together, these test results demonstrate the validity of the three regression models.

Finally, we developed the ENSO reconstruction by merging the three regressions together, with their mean and variance adjusted to be the same as the 1301-1992 nest. The final reconstruction spans 1301-2005, and accounts for 63.5% of instrumental

Niño3.4 SST variance during 1871-1992 when the regression models were built, and 59.5% of variance for the instrumental period 1871-2005 (Fig. 1b). We note that we repeated our analysis by substituting the Niño3.4 index based on the Kaplan SST dataset[11] with that based on the National Climatic Data Center (NCDC) extended reconstructed SST (ERSST) and the Hadley Center SST (HadSST) products[47,48], and found the reconstructions are highly consistent at both high- and low-frequency components (Supplementary Fig. S1). These tests suggest that the PCA-based ENSO reconstruction is not sensitive to the choice of SST products. Here we report the results obtained from the Kaplan SST dataset.

Decadal ENSO variability. Our reconstruction reveals marked decadal variability of the ENSO system over the past seven centuries (Supplementary Fig. S2). Determining the physical cause of such decadal variability is crucial for ENSO diagnosis and prediction. Here we perform cross-wavelet transform to examine whether it was related to cycles of sunspot number[49] (SSN). The results indicate that there exists significant spectral coherence between ENSO and SSN at decadal time scales, but their phase relationships reverse intermittently near-180º over the course of their common period 1749-2005 (Supplementary Fig. S4a). SSN maxima are broadly in phase with warm peaks of decadal ENSO variability in the 1750s-1800s and 1940s-2000s, but are nearly 180º out of phase in the 1850s-1890s and 1910s-1930s. Moreover, the time-varying amplitude between ENSO and solar irradiance has been nonstationary at decadal time scales, broadly consistent in the 1850s-1950s but inconsistent in the 1750s-1840s and the 1960s-2000s (Supplementary Fig. S4b). These observations provide new challenges for the tantalizing

DOI: 10.1038/NCLIMATE1936

sunspot-ENSO relationship at decadal time scales[50,51]. If the 11-year solar cycle is linked to decadal ENSO variability, then the mechanism must be able to accommodate meandering 180º phase reversals through time. Yet, this has not been determined through climate modeling studies. On the other hand, decadal ENSO variability may be internally forced by feedbacks within the coupled ocean-atmosphere system. In that regard, process-oriented model studies are needed to discern feedbacks responsible for such decadal variability. Nonetheless, our 700-year-long ENSO record underlines the significance of decadal variability in the tropical climate. If fully tested in observations and process-oriented model studies, it might lead to significant improvement in decadal climate prediction.

Interdecadal modulation of ENSO variance owing to stochastic noise. Our data indicate substantial interdecadal modulation of ENSO variance and a running variance maximum that coincides with the highest mean state SSTs in the 20th century (Fig. 2a). Here we provide an estimate of the expected range of variability of 31-yr running biweight variance that may arise stochastically through a Monte Carlo approach. From these calculations, we determine if the enhanced ENSO variance in the 20th century exceeds the 95% confidence interval for stochastically-driven running variance.

First, we choose to model the reconstructed ENSO time series as an autoregressive (AR) process, where the AR parameters are estimated through a least squares method[52,53]. We determine the appropriate order of the AR model through optimization based on both the Akaike information criterion (AIC) and the Bayesian information criterion (BIC). Both the AIC and BIC determine the best model as a

second-order autoregressive [AR(2)] model. Thus, the modeled Niño 3.4 SSTs follow the form

$$X_t - \mu = \sum_{k=1}^{2} \varphi_k (X_{t-k} - \mu) + \varepsilon_t, \quad \text{(S1)}$$

where X_t is the Niño 3.4 SST anomaly in year t, μ is the mean Niño 3.4 SST anomaly, φ_k is the autoregressive parameter k, and ε_t is white noise. Here, φ_1 is 0.24, φ_2 is -0.13, and the variance of ε is 0.77 °C^2.

Although ε is specified as white noise, this stochastic component is capable of generating apparent interdecadal modulation of ENSO variance that could be mistaken for a predictable component of interdecadal ENSO variability[18]. In order to determine an estimated 95% confidence interval for 31-yr running biweight variance that may arise stochastically, we employ the following Monte Carlo approach. We generate 10,000 synthetic Niño 3.4 SST anomaly time series according to equation (S1), each of the same length as the reconstructed Niño 3.4 SST time series. For each synthetic time series we calculate 31-yr running biweight variance, just as in Fig. 2a for the actual reconstructed time series. Finally, we calculate the 2.5th and 97.5th percentiles of the running variance from all 10,000 synthetic time series to define a 95% confidence interval. We find that this confidence interval lies between 0.43 and 1.33 °C^2.

There are a few large SST anomalies in the reconstruction (Fig. 1f), raising a possibility that these large outliers are driving interdecadal modulation of ENSO variance. Here we conduct sensitivity tests by artificially suppressing/removing these large SST anomalies. First we identified all events that exceed 2.5 standard deviations (11 cases), artificially reduced their amplitude by 1/2, and then recalculated the 31-yr running biweight variance and the Monte Carlo tests. The variance modulation did not change

DOI: 10.1038/NCLIMATE1936

much, and the 95% confidence interval changed slightly from 0.43-1.33 to 0.38-1.19 °C^2 (Supplementary Fig. S7a). Then we redid the analysis after simply removing the 11 cases that exceed 2.5 standard deviations. The variance results are very similar, and the 95% confidence interval changed a bit to 0.38-1.16 °C^2 (Supplementary Fig. S7b). Together, these tests suggest that the running variances are insensitive to a few large SST anomalies, and that much of the twentieth century ENSO variance stands out from random variability attributable to stochastic processes.

ENSO modulation of NH temperature. Because of poleward transport of anomalous tropical heat, major El Niño events are typically followed by warm hemispheric or global conditions, and vice versa for La Niña events[54]. We test the stationarity of this association using an independent NH temperature reconstruction[9] that was developed with annually resolved records. The correlation between ENSO and NH temperature waxes and wanes over time (Supplementary Fig. S6). Over the past six centuries, every single epoch of elevated ENSO variance is linked to significant correlations between ENSO and NH temperature: in the late fifteenth, early sixteenth, early and late eighteenth century, at the turn of the twentieth century, and in recent decades. This relationship breaks down in the fourteenth century, probably due to the decrease in data quality and quantity[9]. Regardless, the ENSO modulation of NH temperature is consistent with its modulation of pan-Pacific climate over the past seven centuries, suggesting that the modulations are primarily driven by changes in ENSO variance.

Supplementary References

31. Cook, E. R. & Kairiukstis, L. A. *Methods of Dendrochronology.* (Kluwer, 1990).

32. Osborn, T. J., Briffa, K. R. & Jones, P. D. Adjusting variance for sample-size in tree-ring chronologies and other regional mean time series. *Dendrochronologia* **15,** 89–99 (1997).

33. Wigley, T., Briffa, K. R. & Jones, P. D. On the average value of correlated time series, with applications in dendroclimatology and hydrometeorology. *J. Clim. Appl. Meteor.* **23,** 201–213 (1984).

34. Frank, D., Esper, J. & Cook, E. R. On variance adjustments in tree-ring chronology development. In: Heinrich I et al. (Eds.) Tree rings in archaeology, climatology and ecology. *TRACE,* **4,** 56–66 (2006).

35. Cook, E. R. *et al.* Asian monsoon failure and megadrought during the last millennium. *Science* **328,** 486–489 (2010).

36. Cook, E. R. *et al.* Long-term aridity changes in the western United States. *Science* **306,** 1015–1018 (2004).

37. Cook, E. R. *et al.* North American Summer PDSI Reconstructions, Version 2a. IGBP PAGES/World Data Center for Paleoclimatology Data Contribution Series # 2008-046. (2008).

38. Cook, E. R., Seager, R., Cane, M. A. & Stahle, D. W. North American drought: Reconstructions, causes, and consequences. *Earth Sci. Rev.* **81,** 93–134 (2007).

39. Fowler, A. M. *et al.* Multi-centennial tree-ring record of ENSO-related activity in New Zealand. *Nature Clim. Change* **2,** 172–176 (2012).

40. Morales, M. S. *et al.* Precipitation changes in the South American Altiplano since AD

DOI: 10.1038/NCLIMATE1936

1300 reconstructed by tree-rings. Clim. Past **8,** 653–666 (2012).

41. Villalba, R. *et al*. Interdecadal climatic variations in millennial temperature reconstructions from southern South America. *NATO ASI Series I* **41,** 161–189 (1996).

42. Schneider, T. Analysis of incomplete climate data: Estimation of mean values and covariance matrices and imputation of missing values. *J. Climate*, **14**, 853–871 (2001).

43. Wilson, R. *et al.* Reconstructing ENSO: The influence of method, proxy data, climate forcing and teleconnections. *J. Quat. Sci.* **25,** 62–78 (2010).

44. Giese, B. S. & Ray, S. El Niño variability in simple ocean data assimilation (SODA), 1871-2008, *J. Geophys. Res.* **116**, C02024 (2011).

45. Ray, S. & Giese, B. S. Historical changes in El Niño and La Niña characteristics in an ocean reanalysis. *J. Geophys. Res.* **117**, C11007 (2012).

46. Cook, E. R., D'Arrigo, R. & Mann, M. A well-verified, multi-proxy reconstruction of the winter NAO index since AD 1400, *J. Clim.* **15,** 1754–1764 (2002).

47. Smith, T. M., Reynolds, R. W., Peterson, T. C. & Lawrimore, J. Improvements to NOAA's historical merged land-ocean surface temperature analysis (1880-2006). *J. Climate* **21,** 2283–2296 (2008).

48. Rayner, N. A. *et al.* Improved analyses of changes and uncertainties in marine temperature measured in situ since the mid-nineteenth century: the HadSST2 dataset. *J. Climate* **19,** 446–469 (2006).

49. SIDC-team. World Data Center for the Sunspot Index, Royal Observatory of Belgium. *Monthly Report on the International Sunspot Number,* online catalogue of the sunspot index: http://www.sidc.be/sunspot-data/ (1749-2011).

50. Meehl, G. A., Arblaster, J. M., Matthes, K., Sassi F. & van Loon, H. Amplifying the Pacific climate system response to a small 11-year solar cycle forcing. *Science* **325,** 1114–1118 (2009).

51. Meehl, G. A. & Arblaster, J. M. A lagged warm event-like response to peaks in solar forcing in the Pacific region. *J. Climate* **22,** 3647–3660 (2009).

52. Neumaier, A. & Schneider, T. Estimation of parameters and eigenmodes of multivariate autoregressive models. *ACM Trans. Math. Softw.* **27**, 27–57 (2001).

53. Schneider,T. & Neumaier, A. Algorithm 808: ARfit – A Matlab package for the estimation of parameters and eigenmodes of multivariate autoregressive models. *ACM Trans. Math. Softw.* **27**, 58–65 (2001).

54. Jones, P. D. The influence of ENSO on global temperatures. *Climate Monitor.* **17**, 80–89 (1989).

55. Stahle, D.W. *et al.* Experimental dendroclimatic reconstruction of the Southern Oscillation. *Bull. Am. Meteorol. Soc.* **79,** 2137–2152 (1998).

56. D'Arrigo, R., Cook, E. R., Wilson, R. J., Allan, R. & Mann, M. E. On the variability of ENSO over the past six centuries. *Geophys. Res. Lett.* **32**, L03711 (2005).

57. Cook, E. R., D'Arrigo, R. D. & Anchukaitis, K. J. ENSO reconstructions from long tree-ring chronologies: Unifying the differences? Talk presented at a special workshop on "Reconciling ENSO Chronologies for the Past 500 Years", held in Moorea, French Polynesia on April 2-3, 2008.

58. Braganza, K., Gergis, J. L., Power, S. B., Risbey, J. S. & Fowler, A. M. A multiproxy index of the El Nino-Southern Oscillation, A.D. 1525-1982. *J. Geophys. Res.* **114,** D05106 (2009).

DOI: 10.1038/NCLIMATE1936

59. Mann, M. E. *et al*. Global Temperature Patterns in Past Centuries: An Interactive Presentation. *Earth Interactions* **4**, 4 (2000).

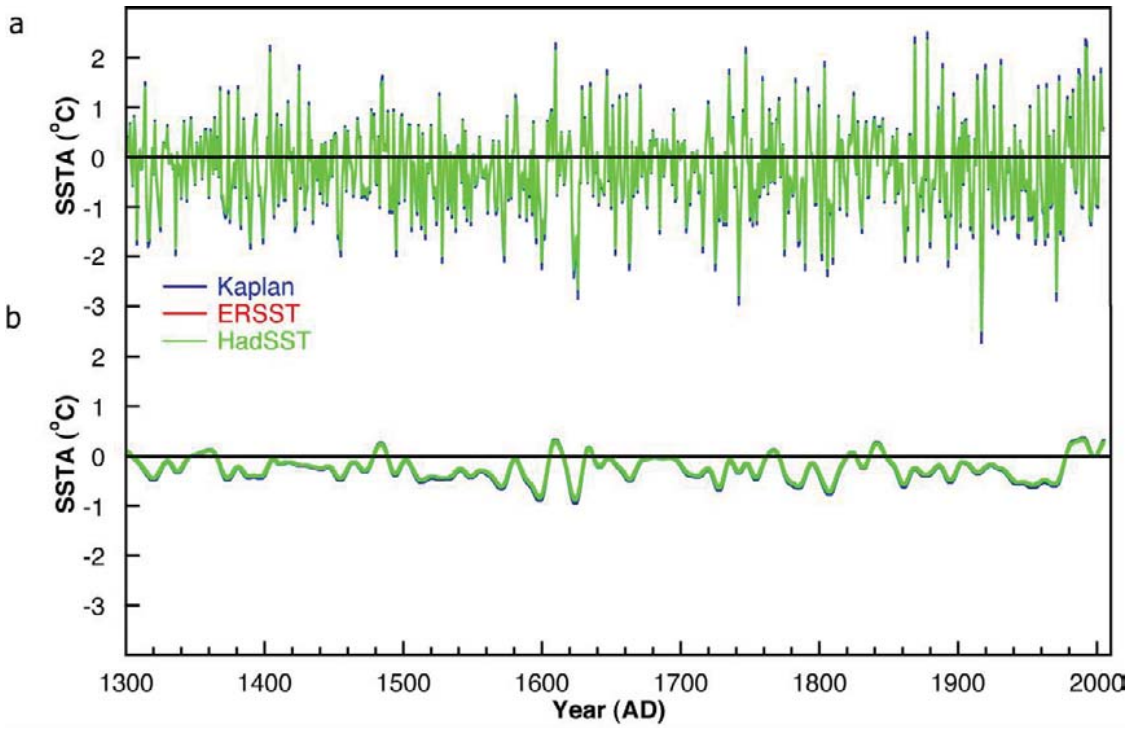

Supplementary Figure S1. a, The reconstructed Niño3.4 SSTs over 1301-2005 by calibration with Kaplan[11] (blue), ERSST[47] (red), and HadSST[48] (green), and **b,** their corresponding 21-yr low-pass filtered SSTs.

DOI: 10.1038/NCLIMATE1936

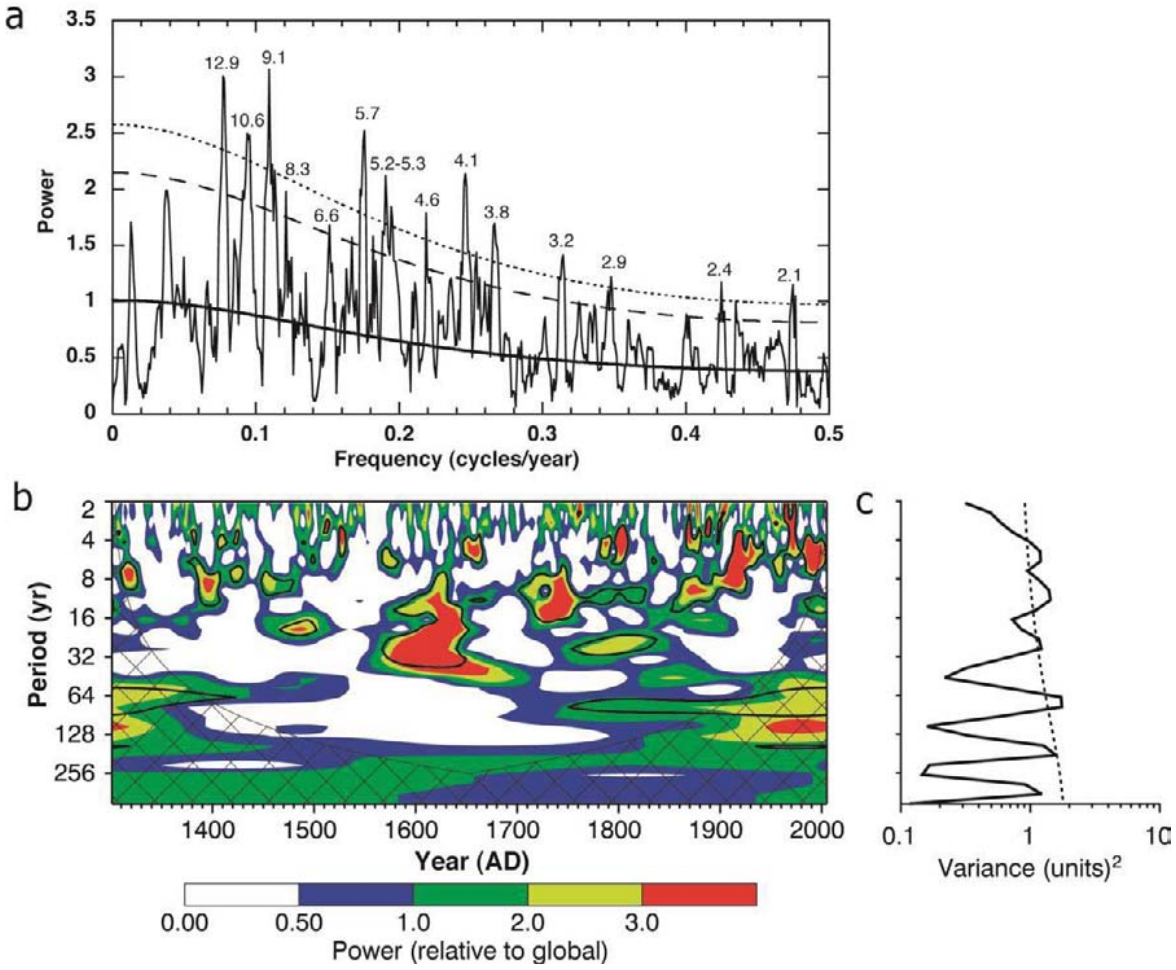

Supplementary Figure S2. Spectral properties of the ENSO reconstruction. **a,** MTM[14] spectral density of the reconstructed Niño3.4 SSTs over 1301-2005. The bold line indicates the corresponding red noise spectrum, and the dashed (dotted) line indicates the 90% (95%) confidence level for a red-noise null hypothesis. **b,** The wavelet power spectrum[15]. The power has been scaled by the global wavelet spectrum. The cross-hatched region is the cone of influence, where zero padding has reduced the variance. Black contour is the 90% confidence level for a red-noise null hypothesis. **c,** The global wavelet power spectrum. The dashed line indicates the 90% confidence level for a red-noise null hypothesis.

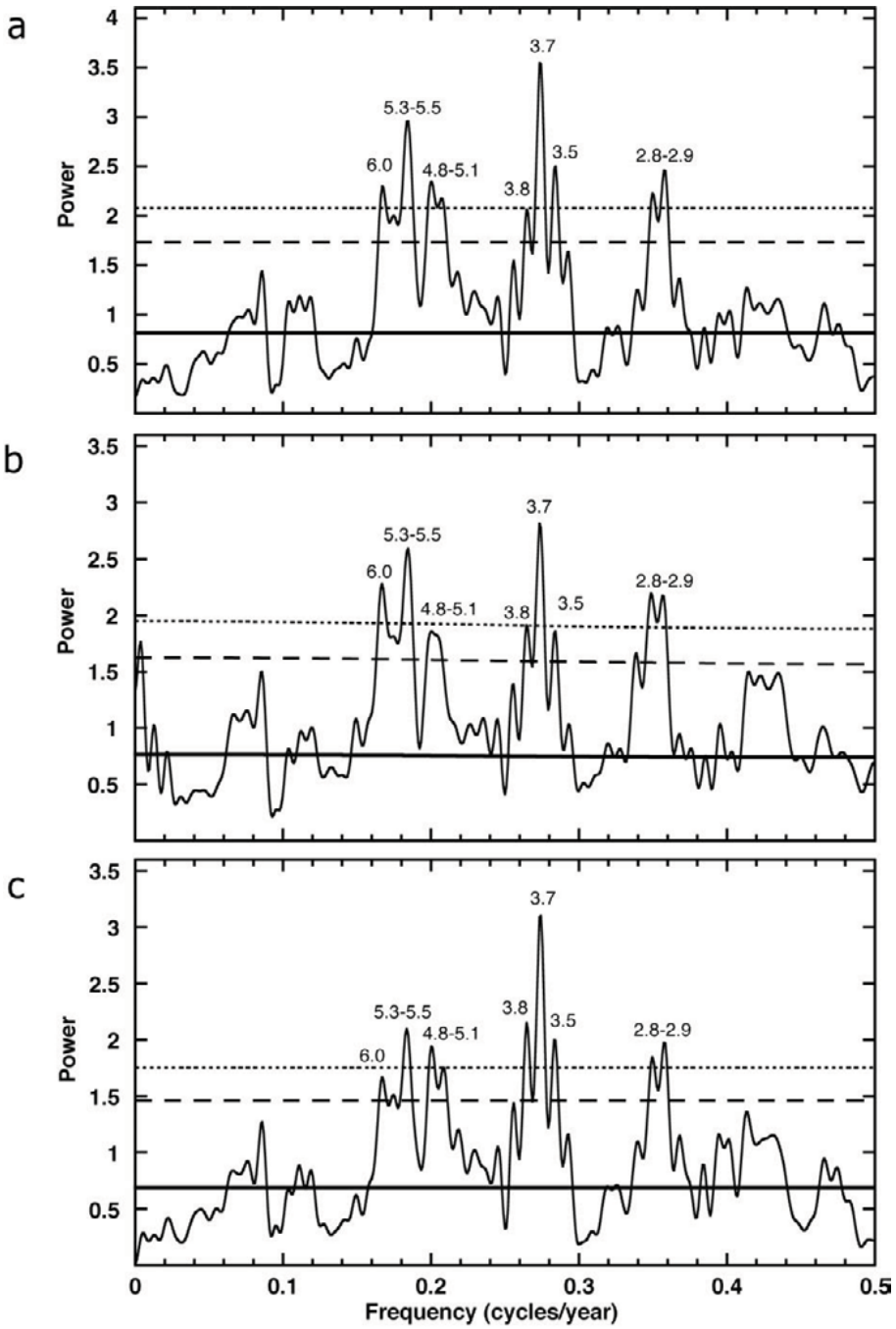

Supplementary Figure S3. MTM[14] spectral density of instrumental Niño3.4 SSTs over 1871-2005 for **a,** Kaplan[11], **b,** ERSST[47], and **c,** HadSST[48]. The bold line indicates the corresponding red noise spectrum, and the dashed (dotted) line indicates the 90% (95%) confidence level for a red-noise null hypothesis.

DOI: 10.1038/NCLIMATE1936

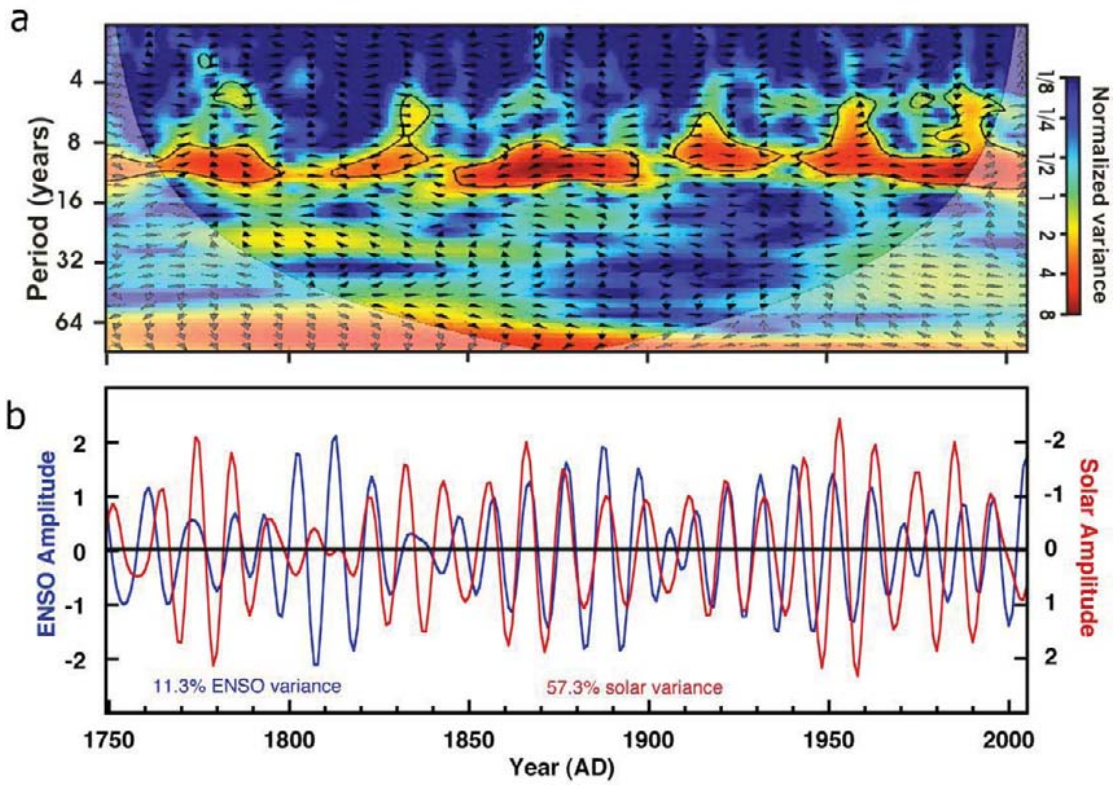

Supplementary Figure S4. Relationship of ENSO with sunspot number. **a,** Cross wavelet transform between the reconstructed Niño3.4 SSTs and the sunspot numbers[49] (March-February) during 1749-2005. Thick black contour indicates the 95% confidence, based on a red noise model. Light shading indicates the cone of influence. Vectors indicate the relative phase relationship between the records, with horizontal arrows pointing right (left) corresponding to in-phase (anti-phase) relationships, respectively. **b,** Comparison between extracted waveforms of decadal ENSO (blue) and solar (red) variability during 1749-2005. Decadal (8-13-yr) variability was extracted using the MTM method[14].

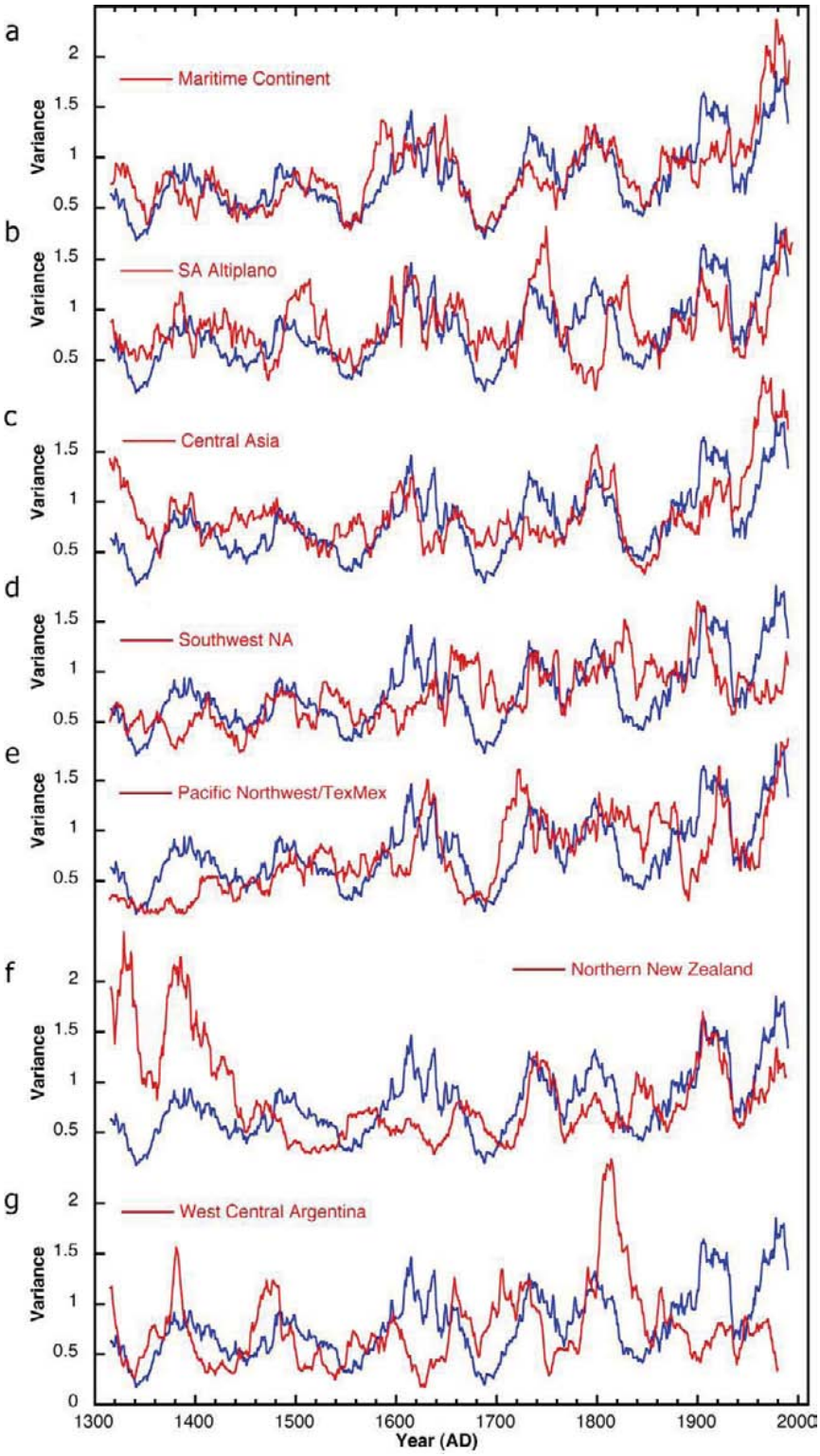

Supplementary Figure S5. Comparison of 31-yr running biweight variance between reconstructed ENSO series (blue) and each time series (red) for **a,** Maritime Continent. **b,** South American Altiplano. **c,** Central Asia. **d,** Southwest North America. **e,** the Pacific Northwest/TexMex region. **f,** northern New Zealand, and **g,** west-central Argentina.

DOI: 10.1038/NCLIMATE1936

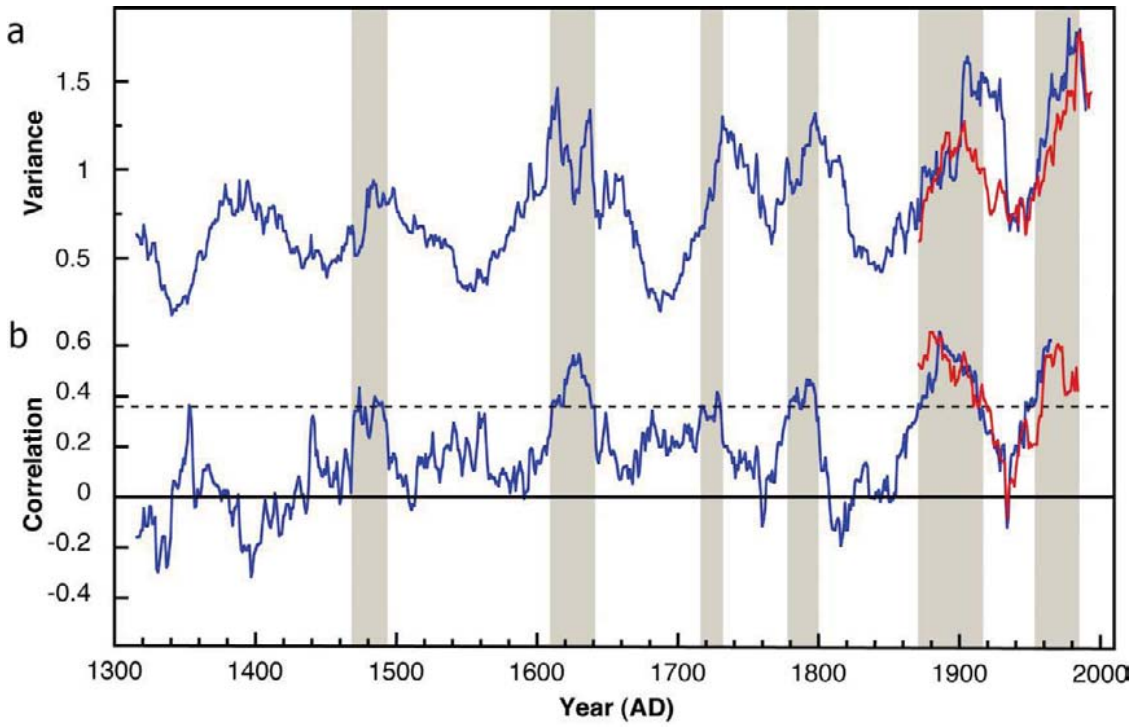

Supplementary Figure S6. ENSO variance and modulation of NH temperature. Comparison of **a,** 31-yr running biweight variance for observed (red) and reconstructed (blue) Niño3.4 SSTs with **b,** 31-yr running correlations of reconstructed Niño3.4 SST with observed (red) and reconstructed (blue) NH temperature[9]. The dashed line in **b** indicates the 0.05 significance level. Vertical shading denotes periods of significant correlations between ENSO and NH temperature.

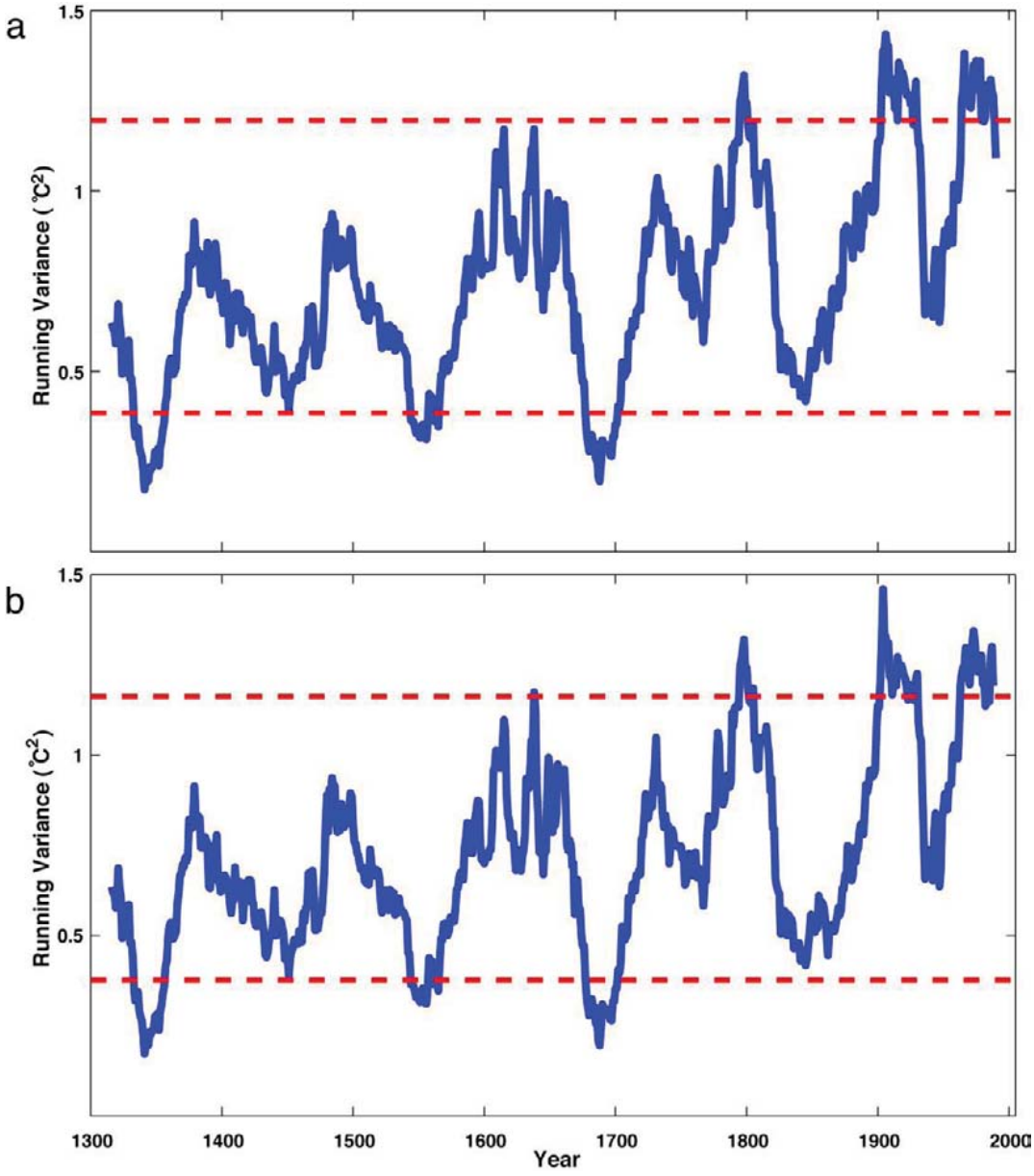

Supplementary Figure S7. Sensitivity tests of ENSO variance change to large SST anomalies. **a,** 31-yr running biweight variance for reconstructed Niño3.4 SSTs with anomalies out of 2.5 standard deviations reduced by 1/2, and **b,** 31-yr running biweight variance for reconstructed Niño3.4 SSTs with anomalies out of 2.5 standard deviations removed. The dashed lines in each panel indicate the 95% confidence interval, based on 10,000 Monte Carlo simulations.

DOI: 10.1038/NCLIMATE1936

Supplementary Table S1. Correlation (*R*) between our new reconstruction and existing ENSO reconstructions (refs. 43, 55-59), along with their explained Niño3.4 SST variance (*Var*) during the common period 1871-1977. Overlapping subset denotes the number of common regions of tree-rings with our reconstruction.

Code	Time Span	*R*	*Var*	Source Region (Overlapping Subset)	Reference
0	1301–2005	1.00	64.5%	Pan-Pacific (7)	This study
1	1706–1977	-0.61	52.0%	Southwest NA (1)	(*55*)
2	1408–1978	0.54	55.8%	Southwest NA (1)	(*56*)
3	1300–1979	0.51	56.3%	Southwest NA (1)	(*57*)
4	1727–1982	-0.60	48.4%	Pacific Basin (2)	(*58*)
5	1525–1982	-0.56	41.2%	Pacific Basin (2)	(*58*)
6	1650–1980	0.48	55.7%	Near Global (3)	(*59*)
7	1540–1998	0.31	31.2%	Tropical Teleconnection (0)	(*43*)

Supplementary Table S2. Descriptive statistics of tree-ring data for ENSO reconstruction.

Code	Data Type[@]	Source Region	Time Interval	ENSO Year[#]	EOF1 Loading[$]	Number of Chronology	Reference
A	MADA PC1	Central Asia	1300–2005	-1/0	0.45	327	*(35)*
B	MADA PC2	Maritime Continent	1300–2005	0/1	-0.54		
C	NADA PC1	Southwest North America	1300–2005	-1/0	0.36	1845	*(36,37)*
D	NADA PC2	Pacific Northwest/ Texas-Mexico	1300–2005	-1/0	-0.23		
E	Regional Chronology	Northern New Zealand	1300–2002	0/1	0.32	38	*(39)*
F	Regional Chronology	South American Altiplano	1300–2009	0/1	0.44	7	*(40)*
G	Regional Chronology	West-central Argentina	1300–1992	-1/0	-0.16	5	*(41)*

[@]MADA and NADA denote Monsoon Asia Drought Atlas and North America Drought Atlas, respectively. [#](-1/0) and (0/1) denote that ENSO events decay and develop in the season of tree growth, respectively. [$]EOF1 Loading for each series during 1301-1992.

DOI: 10.1038/NCLIMATE1936

Supplementary Table S3. Statistics of calibration and verification test results.

	Calibration (1871-1930)	Verification (1931-1992)	Calibration (1931-1992)	Verification (1871-1930)	Full calibration (1871-1992)
r	0.814 0.805 0.781	0.795 0.790 0.780	0.795 0.790 0.780	0.814 0.805 0.781	0.801 0.795 0.779
r^2	0.663 0.648 0.610	0.632 0.624 0.608	0.632 0.624 0.608	0.663 0.648 0.610	0.642 0.632 0.607
RE	—	0.620 0.611 0.597	—	0.647 0.630 0.596	—
CE	—	0.619 0.610 0.596	—	0.646 0.629 0.595	—
Sign test	52+/8- 51+/9- 49+/11-	56+/6- 52+/10- 56+/6-	54+/8- 57+/5- 56+/6-	52+/8- 51+/9- 50+/10-	—

Note: Values in (black; red; blue) denote test results for the regression model ending in (1992; 2003; 2005), respectively. All sign test results are significant at $p<0.001$.

Supplementary Table S4. Summary list of large tropical volcanic events identified for the Superposed Epoch Analysis (SEA). The last column denotes the volcanic explosivity index (VEI) value for each volcanic event. The VEI values are from http://www.volcano.si.edu/world/largeeruptions.cfm.

Volcano Name	Volcanic Subregion	Year	VEI
PINATUBO	Luzon (Philippines)	1991	6
CHICHON, EL	México	1982	5
AGUNG	Lesser Sunda Islands (Indonesia)	1963	5
AMBRYM	Vanuatu	1951	4+
COLIMA	México	1913	5
SANTA MARIA	Guatemala	1902	6?
KRAKATAU	Indonesia	1883	6
COSIGUINA	Nicaragua	1835	5
BABUYAN CLARO	North of Luzon (Philippines)	1831	4?
GALUNGGUNG	Java (Indonesia)	1822	5
TAMBORA	Lesser Sunda Islands (Indonesia)	1815	7
TONGKOKO	Sulawesi (Indonesia)	1680	5?
GAMKONORA	Halmahera (Indonesia)	1673	5?
LONG ISLAND	Northeast of New Guinea	1660	6
PARKER	Philippines - Mindanao	1641	5?
HUAYNAPUTINA	Perú	1600	6
RAUNG	Java (Indonesia)	1593	5?
KELUT	Java (Indonesia)	1586	5?
BILLY MITCHELL	Bougainville Island	1580±20	6
PINATUBO	Luzon (Philippines)	1450±50	5?
CHICHON, EL	México	1360±100	5
COTOPAXI	Ecuador	1350 (?)	4+

DOI: 10.1038/NCLIMATE1936

Supplementary Table S5. Sensitivity tests for ENSO response to tropical eruptions. Values are composite Niño3.4 SST anomalies at each lag, based on the SEA. Asterisk (*) denotes anomalies significant at the 0.01 level, based on a two-tailed student's t-test. Red (blue) color denotes Niño3.4 SST anomalies at the year t=0 (t+1), respectively.

Lag (Year)	VEI>4 (22 events)	VEI>4 (21 events)[@]	VEI>4 (18 events)[#]	VEI>=5 (13 events)	VEI=4 (68 events)
-5	0.242	0.274	0.290	0.383	-0.093
-4	-0.070	-0.054	-0.055	0.028	-0.081
-3	0.094	0.053	0.060	0.029	-0.007
-2	-0.153	-0.146	-0.187	-0.275	0.186
-1	0.032	0.057	0.068	0.133	0.005
0	**-0.423***	**-0.400***	**-0.449***	**-0.533***	**-0.112**
1	**0.610***	**0.629***	**0.624***	**0.717***	**-0.005**
2	0.092	0.064	0.018	0.098	0.096
3	-0.122	-0.167	-0.069	-0.006	-0.057
4	-0.275	-0.256	-0.310	-0.463	0.110
5	-0.249	-0.232	-0.200	-0.183	-0.010

[@]This test excludes the eruption in 1831 (VEI = 4?). [#]This test excludes four eruptions with dating uncertainty (1580, 1450, 1360, 1350).

Supplementary Table S6. Summary list of El Niño and La Niña events during 1950-2005. El Niño and La Niña are defined as the NDJ SST anomalies exceeding 0.5°C, using the 9-yr high-pass filtered Niño3.4 SST index[11].

Event	Year
El Niño	1952, 1958, 1964, 1966, 1969 1970, 1973, 1977, 1983, 1987 1988, 1992, 1995, 1998, 2003
La Niña	1950, 1955, 1956, 1963, 1965 1967, 1968, 1971, 1974, 1976 1981, 1984, 1985, 1986, 1989 1996, 1997, 1999, 2000